PCCP

Confirmation of Gaseous Methanediol from State-of-the-Art Theoretical Rovibrational Characterization

Journal:	*Physical Chemistry Chemical Physics*
Manuscript ID	CP-ART-05-2022-002076.R1
Article Type:	Paper
Date Submitted by the Author:	20-Jul-2022
Complete List of Authors:	Davis, Megan C.; University of Mississippi Garrett, Noah; University of Mississippi Fortenberry, Ryan; University of Mississippi

SCHOLARONE™
Manuscripts

Journal Name

ARTICLE TYPE

Cite this: DOI: 00.0000/xxxxxxxxxx

Confirmation of Gaseous Methanediol from State-of-the-Art Theoretical Rovibrational Characterization†

Megan C. Davis,[a] Noah R. Garrett,[a] and Ryan C. Fortenberry[a‡]

Received Date
Accepted Date

DOI: 00.0000/xxxxxxxxxx

High–level rovibrational characterization of methanediol, the simplest geminal diol, using state-of-the-art, purely *ab initio* techniques unequivocally confirms previously reported gas phase preparation of this simplest geminal diol in its C_2 conformation. The F12-TZ-cCR and F12-DZ-cCR quartic force fields (QFFs) utilized in this work are among the largest coupled cluster-based anharmonic frequencies computed to date, and they match the experimental band origins of the spectral features in the 980-1100 cm^{-1} range to within 3 cm^{-1}, representing a significant improvement over previous studies. The simulated spectrum also matches the experimental spectrum in the strong Q branch feature and qualitative shape of the 980-1100 cm^{-1} region. Additionally, the full set of rotational constants, anharmonic vibrational frequencies, and quartic and sextic distortion constants are provided for both the lowest energy C_2 conformer as well as the slightly higher C_s conformer. Several vibrational modes have intensities of 60 km mol^{-1} or higher, facilitating potential astronomical or atmospheric detection of methanediol or further identification in laboratory work especially now that gas phase synthesis of this molecule has been established.

1 Introduction

Methanediol ($CH_2(OH)_2$), the simplest geminal diol, is a key intermediate in aerosol chemistry.[1,2] It has recently been identified as a key part of formic acid producing pathways ,[3,4] which plays a part in acidification of rainwater[5] and in cloud nucleation[6] The interactions of stable geminal diols with byproducts of Criegee-intermediate formation are, subsequently, likely vital in atmospheric chemistry.[7,8] Astrochemically, methanediol is predicted to be formed on interstellar ice grains[9–11] and goes on to participate in the formation of complex organic molecules.

Despite this importance, methanediol has long been elusive to observe in the gas phase, although it had been experimentally characterized in aqueous solutions,[12–16] through computational modeling,[17–19] and in Ar matrix analysis.[20] Most notably, in 2021, Jian et al. experimentally characterized a portion of the infrared, gas phase spectrum of methanediol[21] through analysis of a mixture of formaldehyde and water vapour in the gas phase. The authors also performed computational analysis to assign features of the resulting spectra using the B3LYP hybrid functional[22,23] with an aug-cc-pVTZ basis set.[24] They assign the O–C–O antisymmetric and symmetric stretches as the origin of the rovibrational feature in the range of 980-1100 cm^{-1}, with experimental band origins at 1580 cm^{-1} and 1027 cm^{-1}, respectively.

Zhu et al. then reported successful synthesis and detection of gaseous methanediol in 2021.[25] Gaseous methanediol is prepared by exposing methanol-oxygen ices to high energy electrons followed by sublimation. Analysis with photoionization-reflectron time-of-flight mass spectrometry subsequently identifies the species together with IR spectroscopy.

Following this, a method for rapid preparation of gaseous methanediol was reported earlier this year by Chen and Chu.[26] An aqueous formaldehyde solution is evaporated allowing for measurement of the IR absorption spectrum of the vapour. The rovibrational feature at 980-1100 cm^{-1} is free from interference of water and formaldehyde, and is identified as methanediol using the computational data from Jian et al. from the experimental band origins and B3LYP/aug-cc-pVTZ rotational parameters. While such theoretical confirmation is common, higher-level methods are really needed in order to verify the spectral features beyond mere empirically-fitted density functional theory results.

The present work utilizes highly accurate *ab initio* QFFs to provide accurate spectroscopic data to comment upon the identification of the 980-1100 cm^{-1} rovibrational feature. High level QFFs based on coupled cluster theory[27–29] produce anharmonic vibrational frequencies that are often within 5 cm^{-1} of experiment and 30 MHz for rotational constants.[30–42] In this work the newly developed F12-TZ-cCR and F12-DZ-cCR QFFs, which produce exceptional accuracies of better even than 1 cm^{-1} for vibrational frequencies in many cases,[43] are utilized to attain this

[a]*Department of Chemistry & Biochemistry, University of Mississippi, University, MS, 38677-1848, USA*
‡*E-mail: r410@olemiss.edu*

† Electronic Supplementary Information (ESI) available: Harmonic vibrational frequencies of C_2 methanediol and data from this work for C_s methanediol. See DOI: 00.0000/00000000.

high accuracy for modest computational cost. The spectroscopic data provided by this work will also aid in possible future detections of methanediol in laboratory synthesis or in the interstellar medium. With the advent of the new approach for synthesizing methanediol in the gas phase from Chen and Chu, these rovibrational spectral data are absolutely essential for complete rovibrational characterization of this molecule.

2 Computational Methods

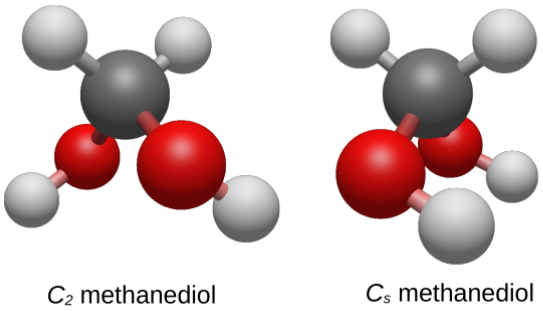

Fig. 1 Structures of methanediol conformers, where red atoms are oxygen, black are carbon and white are hydrogen.

QFFs are utilized in this work in order to efficiently compute the anharmonic vibrational frequencies and other spectroscopic data for both the C_s and C_2 conformations of methanediol (Figure 1). The F12-TZ-cCR and F12-DZ-cCR approaches are utilized as the cheaper and more accurate alternative than other more costly composite QFF methods.[43] These approaches are based on coupled cluster theory at the singles, doubles, and perturbative triples [CCSD(T)] level of theory[27–29] with the explicitly correlated F12b formalism (CCSD(T)-F12b).[44]

First, the geometries for both conformations of methanediol are optimized. The cc-pCVTZ-F12 and cc-pCVDZ-F12 basis sets along with the CCSD(T)-F12b method are employed including core electron correlation for the F12-TZ-cCR and F12-DZ-cCR. Since the F12-DZ-cCR QFF only differs in basis set quality, the double zeta level is used to evaluate the accuracy of a cheaper method and to determine if the double zeta quality can produce accurate results for a lower computational cost. After the optimized geometries are obtained for both conformations, single-point CCSD(T)-F12b energies including core electrons and an additional CCSD(T) Douglas-Kroll scalar relativistic correction[46] are computed for a set of displacements using symmetry internal coordinates. The symmetry internal coordinates for the C_s confirmation of CH_2OH_2 are given in Eqs. 1-15, requiring 19585 total displacements. C_2 methanediol coordinates are given in Eqs. 16-30 and require slightly fewer, specifically 19525 total, displacements to construct the QFF. The H_1 and H_2 atoms are attached to the central carbon atom, and H_3 is attached to O_1 with H_4 attached to O_2. These represent some of the largest coupled cluster-based QFFs computed to date. Additionally, they contain three heavy atoms making them among the most computationally-intensive, large QFFs computed thus far.

Following computation of the single point energies, a least-squares fit is performed to generate force constants, followed by a refit to zero the gradients. INTDER2005[47] is then transforms the force constants from symmetry-internal to Cartesian coordinates. SPECTRO,[48] which uses second–order rotational and vibrational perturbation theory (VPT2),[49–51] is then used in order to calculate the rovibrational spectral data for both conformations of methanediol. Fermi, Coriolis, and Darling-Dennison resonances included in the VPT2 calculations are given in Table S1. Considerations of nuclear spin are left for future work as these would require additional computations beyond the QFFs generated here.

The Molpro quantum chemistry software[45] is used in most cases save for MP2/aug-cc-pVTZ anharmonic intensities from GAUSSIAN16.[52] From these data, theoretical spectra is generated with PGOPHER,[53] using a Gaussian value of 0.45 cm^{-1} for the line widths and using relative anharmonic intensities and other spectral data calculated herein. The simulation is performed at 298 K similar to the experimental conditions of Chen and Chu.[26]

$$S_1(a') = H_1 - C \quad (1)$$

$$S_2(a') = H_2 - C \quad (2)$$

$$S_3(a') = (O_1 - C) + (O_2 - C) \quad (3)$$

$$S_4(a') = (O_1 - H_3) + (O_2 - H_4) \quad (4)$$

$$S_5(a') = \angle(H_1 - C - H_2) \quad (5)$$

$$S_6(a') = \angle(O_1 - C - H_1) + \angle(O_2 - C - H_1) \quad (6)$$

$$S_7(a') = \angle(C - O_1 - H_3) + \angle(C - O_2 - H_4) \quad (7)$$

$$S_8(a'') = \tau(O_1 - C - H_1 - H_2) - \tau(O_2 - C - H_1 - H_2) \quad (8)$$

$$S_9(a'') = \tau(H_3 - O_1 - C - H_1) - \tau(H_4 - O_2 - C - H_2) \quad (9)$$

$$S_{10}(a'') = (C - O_1) - (C - O_2) \quad (10)$$

$$S_{11}(a'') = (O_1 - H_3) - (O_2 - H_4) \quad (11)$$

$$S_{12}(a'') = \angle(O_1 - C - H_1) - \angle(O_2 - C - H_1) \quad (12)$$

$$S_{13}(a'') = \angle(C - O_1 - H_3) - \angle(C - O_2 - H_4) \quad (13)$$

$$S_{14}(a') = \tau(O_1 - C - H_1 - H_2) + \tau(O_2 - C - H_1 - H_2) \quad (14)$$

$$S_{15}(a') = \tau(H_3 - O_1 - C - H_1) + \tau(H_4 - O_2 - C - H_1) \quad (15)$$

Table 1 C_2 Methanediol Anharmonic Vibrational Frequencies in cm^{-1}

		F12-XZ-cCR			Jian et al.[21]		Lugez et al.[‡20]	Barrientos et al.[17]	
Mode	Description	TZ	DZ	Int.[†]	B3LYP	Gas Phase	Argon Matrix	MP2	QCISD
$\nu_1(a)$	sym. OH stret.	3647.6	3651.4	30	3617		3638.8-3637.6	3648	3711
$\nu_2(b)$	anti. OH stret.	3647.9	3651.7	50	3612		3564.4	3648	3710
$\nu_3(b)$	anti. CH stret.	2978.4	2978.6	33	2937		2977.7	3020	3007
$\nu_4(a)$	sym. CH stret.	2923.3	2929.3	31	2897			2807	2956
$\nu_5(a)$	CH_2 sciss.	1503.6	1505.4	1	1486			1374	1498
$\nu_6(b)$	CH_2 wag.	1404.5	1414.0	30	1413		1425.7-1424.4	1441	1413
$\nu_7(a)$	CH_2 twist	1351.4	1358.6	2	1354		1358.7-1353.8	1350	1360
$\nu_8(b)$	anti. COH bend	1334.2	1339.4	18	1311		1334.6	1329	1341
$\nu_9(a)$	sym. COH bend	1198.7	1196.5	2	1176			1188	1178
$\nu_{10}(b)$	anti. OCO stret.	1060.5	1060.7	267	1012	1058	1056.5-1055.4	1048	1070
$\nu_{11}(a)$	sym. OCO stret.	1029.3	1028.3	95	1003	1027		1019	1024
$\nu_{12}(b)$	CH rock	1013.3	1010.9	18	1006			1010	985
$\nu_{13}(a)$	OCO bend	544.1	545.4	50	554		547.7-545.4	538	545
$\nu_{14}(a)$	sym. COH torsion	358.6	366.4	64	376			368	366
$\nu_{15}(b)$	anti. COH torsion	325.0	333.0	149	367			333	349

†Anharmonic intensities given in km mol^{-1} calculated at the MP2/aug-cc-pVTZ level
‡Assignments given here differ from those originally estimated by Lugez et al.

$$S_1(b) = (C-H_1)+(C-H_2) \quad (16)$$

$$S_2(a) = (C-O_1)+(C-O_2) \quad (17)$$

$$S_3(a) = (O_1-H_3)+(O_2-H_4) \quad (18)$$

$$S_4(b) = \angle(H_1-C-H_2) \quad (19)$$

$$S_5(a) = \angle(O_1-C-H_1)+\angle(O_2-C-H_2) \quad (20)$$

$$S_6(b) = \angle(C-O_1-H_3)+\angle(C-O_2-H_4) \quad (21)$$

$$S_7(a) = \tau(O_1-C-H_1-H_2)+\tau(O_2-C-H_2-H_1) \quad (22)$$

$$S_8(b) = \tau(H_3-O_1-C-H_1)+\tau(H_4-O_2-C-H_2) \quad (23)$$

$$S_9(a) = (C-H_1)-(C-H_2) \quad (24)$$

$$S_{10}(b) = (C-O_1)-(C-O_2) \quad (25)$$

$$S_{11}(a) = (O_1-H_3)-(O_2-H_4) \quad (26)$$

$$S_{12}(a) = \angle(O_1-C-H_1)-\angle(O_2-C-H_2) \quad (27)$$

$$S_{13}(b) = \angle(C-O_1-H_3)-\angle(C-O_2-H_4) \quad (28)$$

$$S_{14}(b) = \tau(O_1-C-H_1-H_2)-\tau(O_2-C-H_2-H_1) \quad (29)$$

$$S_{15}(a) = \tau(H_3-O_1-C-H_1)-\tau(H_4-O_2-C-H_2) \quad (30)$$

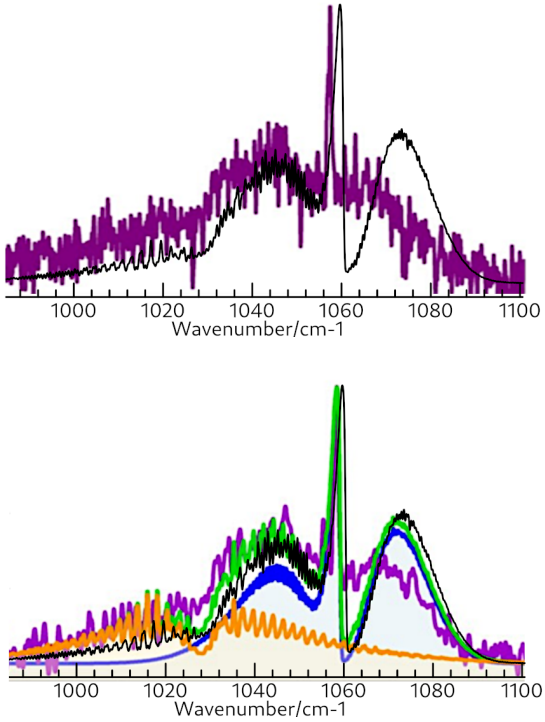

Fig. 2 Convolved F12-TZ-cCR spectra (black) from the corresponding ν_{10} (blue) and ν_{11} (orange) features overlaid with experimental spectra (purple) and B3LYP (green) from Chen and Chu[26].

3 Results and discussion

The simulated, pure *ab initio* F12-TZ-cCR spectra for the combined ν_{10} and ν_{11} C=O antisymmetric and symmetric stretches, respectively, (including the vibrationally–averaged rotational constants of both fundamentals) for the C_2 conformation of methanediol is shown in Figure 2. In the top portion, the black computed spectrum almost exactly matches the experimental IR data of Chen and Chu for this rovibrational feature in the 980-1100 cm^{-1} range.[26] This provides unambiguous confirmation of Chen and Chu's successful preparation of methanediol in the gas-phase. The F12-TZ-cCR spectrum additionally matches with the authors' previous spectrum produced with experimental band origins and B3LYP/aug-cc-pVTZ rotational constants, also shown in green in the bottom of Figure 2. The strong Q branch feature arising from the a-type ν_{10} transition as well as the shoulder from approximately 980 cm^{-1} to 1060 cm^{-1}, consisting of both the P branch of ν_{10} and the b-type ν_{11} rovibrational feature, strongly support this feature arising from the presence of methanediol. The individual contributions from the ν_{10} and ν_{11} features to the overall

spectrum can be seen in the blue and orange traces in the bottom of Figure 2 as well as in Figure S1[†] Only the C_2 conformation is considered in the spectral simulation, as the relative, anharmonic, zero-point energy-corrected energy between the two conformers is calculated to be 781.28 cm^{-1} at the F12-TZ-cCR level, resulting in a negligible Boltzmann ratio of 0.02 for C_s relative to C_2 at 298 K imply that the C_s form will have no observeable contribution to the spectrum generated previously.

Table 2 C_2 Methanediol Rotational Constants in MHz

	F12-cCR		Jian et al.[21]	Barrientos et al.[17]
Parameter	TZ	DZ	B3LYP	CCSD(T)/aVTZ
A_e	42038.1	42001.5	41973.9	41669.1
B_e	10290.7	10272.4	10118.0	10183.5
C_e	9112.2	9097.8	8981.8	9017.7
A_0	41613	41566.3	41548.2	
B_0	10205.8	10190.5	10043.0	
C_0	9018	9004.8	8891.8	
A_1	41473.2	41426.8		
B_1	10204.7	10189.5		
C_1	9015.6	9002.5		
A_2	41467.1	41421.7		
B_2	10204.8	10189.6		
C_2	9015.5	9002.4		
A_3	41547.3	41500.3		
B_3	10219.7	10204.6		
C_3	9026.1	9013		
A_4	41500.9	41454.2		
B_4	10212.1	10196.9		
C_4	9024.7	9011.5		
A_5	41520.8	41474.4		
B_5	10193.4	10178.1		
C_5	9009.4	8996.3		
A_6	41566.6	41519.7		
B_6	10211.6	10196.1		
C_6	9012.5	8999.3		
A_7	41645.8	41595.7		
B_7	10204.4	10189		
C_7	9048.9	9034.8		
A_8	41511.7	41464		
B_8	10206.7	10191.8		
C_8	8982.2	8969.9		
A_9	41537	41489.4		
B_9	10188.1	10173.4		
C_9	9006.5	9003.2		
A_{10}	41298.8	41254.2	41254.4	
B_{10}	10147.6	10132.5	10004.1	
C_{10}	8968.2	8955.2	8828.9	
A_{11}	41692.5	41657.6	41734.1	
B_{11}	10162.5	10147.2	9998.1	
C_{11}	8986.7	8973.6	8870.9	
A_{12}	41403	41345.3		
B_{12}	10176.8	10161.5		
C_{12}	8990.2	8967.2		
A_{13}	41822.4	41774.6		
B_{13}	10174.4	10159.5		
C_{13}	8984.4	8971.3		
A_{14}	41958.6	41908.9		
B_{14}	10185.7	10175.9		
C_{14}	9002.8	8991.5		
A_{15}	41399.8	41336.9		
B_{15}	10224.8	10208.8		
C_{15}	9008.4	8994.6		

Additionally, the calculated frequency of the ν_{10} antisymmetric O–C–O stretch at 1060.7 cm^{-1}, given in Table 1, lines up almost exactly with the experimental data of Jian et. al. at 1058 cm^{-1}.[21] This is a significant improvement over the previous B3LYP/aug-cc-pVTZ computations, which place the ν_{10} frequency at 1012 cm^{-1} before empirical correction. The F12-TZ-cCR QFF VPT2 ν_{11} symmetric O–C–O stretch at 1028.3 cm^{-1} also agrees excellently with the experimental value of 1027 cm^{-1}. The purely uncorrected, *ab initio* F12-TZ-cCR data produced in this work, furthermore, agrees significantly more closely with Jian et al.'s experimental data than does the previous theoretical work given in Table 1 utilized to confirm the gas phase presence of methanediol. The other, previous, scaled harmonic QCISD work of Barrientos et al.[17] places ν_{10} at 1070 cm^{-1} and ν_{11} at 1024 cm^{-1}, which are the closest values from previous theory even though they are 10 cm^{-1} and 3 cm^{-1} away from experiment, respectively.

F12-TZ-cCR also compares well with the Argon matrix data from Lugez et al.[20] The ν_3 frequency agrees within 1 cm^{-1}, as does the ν_8 frequency. The ν_{10}, ν_{13}, and ν_2 frequencies agree to within 4 cm^{-1}. The other fundamental frequencies agree reasonably, with the largest difference being the ν_6 frequency with a difference of 20.1 cm^{-1} from the experimental lower bound. Agreement is generally closer between the Argon matrix data and that from the F12-TZ-cCR QFF than any previous theory, with a couple of exceptions. For the ν_7 mode, the scaled QCISD data of Barrientos et al. matches 1.1 cm^{-1} more closely to the upper bound than F12-TZ-cCR does to the lower bound. Similarly, for the ν_{13} mode the QCISD data matches more closely by 0.9 cm^{-1}. The QCISD data and Jian et al.'s B3LYP data are approximately 10 cm^{-1} closer for the ν_6 mode, also. However, no other data are as consistently representative as that reported herein implying that this full set of fundamental, anharmonic frequencies are the most accurate produced to date.

Table 3 C_2 Methanediol Distortion Constants

Parameter	Units	F12-TZ-cCR	F12-DZ-cCR
Δ_J	kHz	10.924	10.904
Δ_K	kHz	417.637	418.185
Δ_{JK}	MHz	-0.0516	-0.0517
δ_J	kHz	2.274	2.272
δ_{JK}	kHz	23.341	23.353
Φ_J	mHz	22.93	23.518
Φ_K	Hz	15.352	15.307
Φ_{JK}	mHz	97.769	95.849
Φ_{KJ}	Hz	-3.604	-3.599
ϕ_j	mHz	10.361	10.651
ϕ_{jk}	mHz	147.597	160.424
ϕ_k	Hz	6.6	6.85
μ_y	D	0.06	
μ	D	0.06	

Table 4 C_2 Methanediol Geometry

Parameter	Units	F12-TZ-cCR	F12-DZ-cCR
r_0(C1-H2/3)	Å	1.100	1.100
r_0(C1-O4/5)	Å	1.409	1.410
r_0(O4-H6)	Å	0.949	0.949
r_0(O5-H7)	Å	0.949	0.949
$\angle_0$(C1-H2-H3)	deg	109.945	109.932
$\angle_0$(C1-O4-H2)	deg	111.775	111.777
$\angle_0$(C1-O5-H3)	deg	111.775	111.777
$\angle_0$(O4-C1-H6)	deg	108.266	108.158
$\angle_0$(O5-C1-H7)	deg	108.266	108.158

Rotational constants from this work and previous theory are given in Table 2. Similar agreement is seen across levels of theory, but the F12-TZ-cCR values are known to be within 7.5 MHz (0.05%) of experiment implying that these computed herein should be exceptionally reliable.[43] Additionally, the vibrationally-averaged rotational constants are provided herein for every vibrational mode by the F12-XZ-cCR theories. Distortion constants are also give in Table 3, providing the means to simulate accurate spectra for additional rovibrational features of methanediol.

The ν_{10} and ν_{11} frequencies have the highest intensities for the C_2 conformation, at 95 and 267 km mol^{-1}, thus the previously reported rovibrational feature at 980-1100 cm^{-1} will likely be the most significant fingerprint for gas phase methanediol. The ν_{14} and ν_{15} frequencies have respectable intensities at 64 and 149 km mol^{-1}, respectively, providing an additional means of detecting this molecule in the far infrared/terahertz region.

Table 5 gives anharmonic vibrational frequencies for the C_s conformation of methanediol. This conformation, although higher in energy, has a significantly higher dipole moment of 2.72 D (Table S6†) compared to the 0.055 D dipole moment of the C_2 conformation, potentially rendering it detectable in the microwave region if present in high enough concentrations. It also has several bright intensity fundamental vibrational frequencies which may give rise to distinct spectral features at high temperatures. The ν_{10} and ν_{14} frequencies are exceptionally bright, with intensities of 237 km mol^{-1} and 112 km mol^{-1}, respectively, and the ν_{15} frequency has a respectable intensity of 64 km mol^{-1}. Looking at F12-TZ-cCR, the ν_{10} frequency of the C_s conformation is shifted by 5.2 cm^{-1} from the corresponding frequency of the C_2 conformation, while the ν_{11} frequency has a negligible intensity of 26 km mol^{-1}. This may result in potential, high-temperature astronomical spectra presenting a less prominent shoulder than seen in the 980-1060 cm^{-1} region of Figure 2 for the C_2 conformation. The ν_{14} frequency has a nearly overlapping origin with the ν_{15} frequency of the C_2 conformation, at 336.2 cm^{-1} compared to 332.5 cm^{-1} for F12-TZ-cCR, which may result in an appreciable change of this feature at high temperatures. Frequencies from previous theoretical work are also given in Table 5 for the C_s conformation. Additionally, rotational constants, distortion constants and geometrical parameters are given in Tables S5† and S6†, allowing for modelling of spectra for this conformation.

Comparison between F12-TZ-cCR and F12-DZ-cCR is quite favorable for the latter for both conformations. For the C_2 conformer, the anharmonic vibrational frequencies have a mean absolute difference (MAD) of 4.0 cm^{-1}. The bright ν_{10} and ν_{11} frequencies have a difference of 0.2 cm^{-1} and 1.0 cm^{-1}, respectively. Similarly, the rotational constants for F12-DZ-cCR have an MAD of 25.2 MHz relative to F12-TZ-cCR. The geometries for each method, given in Table 4, are nearly identical. Distortion constants, given in Table 3 also compare reasonably, with the possible exception of the ϕ_{jk} constant, with a difference of 12.827 mHz between the two methods.

In comparing F12-TZ-cCR and F12-DZ-cCR for the C_s conformation, the vibrational frequencies have an MAD of 3.4 cm^{-1}. The bright intensity ν_{10}, ν_{11}, and ν_{14} frequencies differ by 1 cm^{-1} or less between the two methods, although the reasonably intense ν_{15} frequency is 12.2 cm^{-1} higher for F12-DZ-cCR, which is the largest discrepancy between the two QFFs. The geometries, given in Table S4† are virtually identical. The distortion constants are similar with the exception of the Δ_{JK} constant, which is 2.816 kHz for F12-TZ-cCR versus 4.906 kHz for F12-DZ-cCR. The rotational constants between the two methods have an MAD of 25.5 MHz for the C_s conformation.

4 Conclusion

Simulated spectra from state-of-the-art, purely *ab initio* F12-TZ-cCR QFFs confirm the assignment of the 980-1100 cm^{-1} rovibrational feature reported by Chen and Chu[26] as arising from gaseous methanediol. The unadulterated F12-TZ-cCR rovibrational spectrum matches exceptionally well with the experimentally observed spectral features arising from the ν_{10} and ν_{11} vibrational transitions, and agrees with the experimental band origins to within 3 cm^{-1}. Additional rovibrational data is also provided in order to produce a complete rovibrational spectral characterization of this molecule in both C_2 and C_s conformations. Most notably, the C_s conformation, lying only 781 cm^{-1} (9.34 kJ mol^{-1}) above the 0.055 D C_2, has a much larger dipole moment at 2.72 D implying that microwave studies and radioastronomical observations would be more likely to find this higher-energy C_s conformer than the C_2. The F12-DZ-cCR approach is additionally shown to achieve excellent accuracy relative to the more costly F12-TZ-cCR, with an MAD of 4.0 cm^{-1} relative to the latter for vibrational frequencies and 25.2 MHz for rotational constants for the C_2 conformation. The data provided herein should serve to facilitate possible future astronomical or atmospheric detection of methanediol as well as further classification and examination in the laboratory.

Author Contributions

Megan C. Davis was responsible for spectral simulations, writing the original draft and supervision. Noah R. Garrett was responsible for investigation via performing theoretical calculations and contributed to the original draft. Ryan C. Fortenberry was responsible for conceptualization, project administration, and supervision, as well as review and editing for the manuscript.

Conflicts of interest

There are no conflicts of interest to declare.

Acknowledgements

Funding is acknowledged from NSF grant NSF-1757220 for support of MCD, NASA grant NNX17AH15G for support of RCF, and start-up funds provided by the University of Mississippi for all three authors. Additionally, the computing resources were provided in part by the Mississippi Center for Supercomputing Research funded with contributions from NSF grant CHE-1757888.

Table 5 C_s Methanediol Anharmonic Vibrational Frequencies in cm^{-1}

		F12-XZ-cCR			Jian et al.[21]	Barrientos et al.[17]	
Mode	Description	TZ	DZ	Int.†	B3LYP	MP2	QCISD
$\nu_1(a'')$	anti. OH stret.	3665.3	3668.4	20	3623	3669	3725
$\nu_2(a')$	sym. OH stret.	3662.5	3665.8	47	3622	3667	3724
$\nu_3(a')$	CH_2 stret.	2995.1	2993.3	21	2980	3053	3042
$\nu_4(a')$	CH_1 stret.	2885.1	2890.2	47	2864	2846	2926
$\nu_5(a')$	CH_2 sciss.	1495.3	1499.5	1	1478	1451	1487
$\nu_6(a'')$	CH_2 wag	1408.1	1414.9	20	1404	1416	1405
$\nu_7(a')$	CH_2 twist	1372.2	1370.9	17	1363	1359	1380
$\nu_8(a'')$	COH bend	1344.6	1342.5	1	1320	1336	1343
$\nu_9(a'')$	COH bend	1140.3	1142.8	55	1149	1131	1138
$\nu_{10}(a'')$	anti. OCO stret.	1055.3	1054.3	237	1029	1040	1065
$\nu_{11}(a')$	sym. OCO stret.	1055.4	1052.4	26	1004	1048	1044
$\nu_{12}(a')$	CH_2 rock	997.1	999.2	54	980	995	976
$\nu_{13}(a')$	OCO bend	537.0	535.2	11	526	530	525
$\nu_{14}(a')$	sym. COH torsion	336.2	336.5	112	307	331	363
$\nu_{15}(a'')$	anti. COH torsion	119.6	131.8	64	63	112	155

†Anharmonic intensities given in km mol^{-1} calculated at the MP2/aug-cc-pVTZ level

Notes and references

1 J. L. Axson, K. Takahashi, D. O. D. Haan and V. Vaida, *Proceedings of the National Academy of Sciences*, 2010, **107**, 6687–6692.

2 M. K. Hazra, J. S. Francisco and A. Sinha, *The Journal of Physical Chemistry A*, 2014, **118**, 4095–4105.

3 B. Franco, T. Blumenstock, C. Cho, L. Clarisse, C. Clerbaux, P. F. Coheur, M. D. Mazière, I. D. Smedt, H. P. Dorn, T. Emmerichs, H. Fuchs, G. Gkatzelis, D. W. T. Griffith, S. Gromov, J. W. Hannigan, F. Hase, T. Hohaus, N. Jones, A. Kerkweg, A. Kiendler-Scharr, E. Lutsch, E. Mahieu, A. Novelli, I. Ortega, C. Paton-Walsh, M. Pommier, A. Pozzer, D. Reimer, S. Rosanka, R. Sander, M. Schneider, K. Strong, R. Tillmann, M. V. Roozendael, L. Vereecken, C. Vigouroux, A. Wahner and D. Taraborrelli, *Nature*, 2021, **593**, 233–237.

4 J. de Gouw and D. Farmer, *Nature*, 2021, **593**, 198–199.

5 W. L. Chameides and D. D. Davis, *Nature*, 1983, **304**, 427–429.

6 S. Yu, *Atmospheric Research*, 2000, **53**, 185–217.

7 O. Welz, J. D. Savee, D. L. Osborn, S. S. Vasu, C. J. Percival, D. E. Shallcross and C. A. Taatjes, *Science*, 2012, **335**, 204–207.

8 M. I. Lester and S. J. Klippenstein, *Accounts of Chemical Research*, 2018, **51**, 978–985.

9 R. T. Garrod, S. L. W. Weaver and E. Herbst, *The Astrophysical Journal*, 2008, **682**, 283–302.

10 W. A. Schutte, L. J. Allamandola and S. A. Sandford, *Icarus*, 1993, **104**, 118–137.

11 F. Duvernay, A. Rimola, P. Theule, G. Danger, T. Sanchez and T. Chiavassa, *Phys. Chem. Chem. Phys.*, 2014, **16**, 24200–24208.

12 H. Matsuura, M. Yamamoto and H. Murata, *Spectrochimica Acta Part A: Molecular Spectroscopy*, 1980, **36**, 321–327.

13 G. I. M. V. D. O. G. F. Ryabova, R. S.; Voloshenko, *Russian Journal of Applied Chemistry*, 2002, **75**, 22–24.

14 K. Z. Gaca-Zajac, B. R. Smith, A. Nordon, A. J. Fletcher, K. Johnston and J. Sefcik, *Vibrational Spectroscopy*, 2018, **97**, 44–54.

15 N. Lebrun, P. Dhamelincourt, C. Focsa, B. Chazallon, J. L. Destombes and D. Prevost, *Journal of Raman Spectroscopy*, 2003, **34**, 459–464.

16 G. R. Möhlmann, *Journal of Raman Spectroscopy*, 1987, **18**, 199–203.

17 C. Barrientos, P. Redondo, H. Martínez and A. Largo, *The Astrophysical Journal*, 2014, **784**, 132.

18 P. Delcroix, M. Pagliai, G. Cardini, D. Bégué and B. Hanoune, *The Journal of Physical Chemistry A*, 2015, **119**, 290–298.

19 B. M. Hays and S. L. W. Weaver, *The Journal of Physical Chemistry A*, 2013, **117**, 7142–7148.

20 C. Lugez, A. Schriver, R. Levant and L. Schriver-Mazzuoli, *Chemical Physics*, 1994, **181**, 129–146.

21 H.-Y. Jian, C.-T. Yang and L.-K. Chu, *Physical Chemistry Chemical Physics*, 2021, **23**, 14699–14705.

22 A. D. Becke, *J. Chem. Phys.*, 1993, **98**, 5648–5652.

23 C. T. Lee, W. T. Yang and R. G. Parr, *Phys. Rev. B.*, 1988, **37**, 785–789.

24 T. H. Dunning, *J. Chem. Phys.*, 1989, **90**, 1007–1023.

25 C. Zhu, N. F. Kleimeier, A. M. Turner, S. K. Singh, R. C. Fortenberry and R. I. Kaiser, *Proceedings of the National Academy of Sciences*, 2021, **119**, e2111938119.

26 Y.-F. Chen and L.-K. Chu, *Chemical Communications*, 2022, **58**, 4208–4210.

27 K. Raghavachari, G. W. Trucks, J. A. Pople and M. Head-Gordon, *Chem. Phys. Lett.*, 1989, **157**, 479–483.

28 I. Shavitt and R. J. Bartlett, *Many-Body Methods in Chemistry and Physics: MBPT and Coupled-Cluster Theory*, Cambridge University Press, Cambridge, 2009.

29 T. D. Crawford and H. F. Schaefer III, in *Reviews in Computational Chemistry*, ed. K. B. Lipkowitz and D. B. Boyd, Wiley, New York, 2000, vol. 14, pp. 33–136.

30 X. Huang, P. R. Taylor and T. J. Lee, *J. Phys. Chem. A*, 2011, **115**, 5005–5016.

31 R. C. Fortenberry, X. Huang, J. S. Francisco, T. D. Crawford and T. J. Lee, *J. Chem. Phys.*, 2012, **136**, 234309.

32 R. C. Fortenberry, X. Huang, J. S. Francisco, T. D. Crawford and T. J. Lee, *J. Phys. Chem. A.*, 2012, **116**, 9582–9590.

33 D. Zhao, K. D. Doney and H. Linnartz, *Astrophys. J. Lett.*, 2014, **791**, L28.

34 W. J. Morgan and R. C. Fortenberry, *J. Phys. Chem. A*, 2015, **119**, 7013–7025.

35 R. A. Theis and R. C. Fortenberry, *Molec. Astrophys.*, 2016, **2**, 18–24.

36 L. Bizzocchi, V. Lattanzi, J. Laas, S. Spezzano, B. M. Giuliano, D. Prudenzano, C. Endres, O. Sipilä and P. Caselli, *Astron. Astrophys.*, 2017, **602**, A34.

37 M. J. R. Kitchens and R. C. Fortenberry, *Chem. Phys.*, 2016, **472**, 119–127.

38 R. C. Fortenberry and J. S. Francisco, *Astrophys. J.*, 2017, **835**, 243.

39 A. Fuente, J. R. Goicoechea, J. Pety, R. L. Gal, R. Martín-Doménech, P. Gratier, V. Guzmán, E. Roueff, J. C. Loison, G. M. M. Caro, V. Wakelam, M. Gerin, P. Riviere-Marichalar and T. Vidal, *Astrophys. J. Lett*, 2017, **851**, 49.

40 J. P. Wagner, D. C. McDonald II and M. A. Duncan, *Angew. Chem. Int. Ed*, 2018, **57**, 5081–5085.

41 R. C. Fortenberry and T. J. Lee, *Ann. Rep. Comput. Chem.*, 2019, **15**, 173–202.

42 M. B. Gardner, B. R. Westbrook, R. C. Fortenberry and T. J. Lee, *Spectrochim. Acta A*, 2021, **248**, 119184.

43 A. G. Watrous, B. R. Westbrook and R. C. Fortenberry, *The Journal of Physical Chemistry A*, 2021, **125**, 10532–10540.

44 T. B. Adler, G. Knizia and H.-J. Werner, *J. Chem. Phys.*, 2007, **127**, 221106.

45 H. J. Werner, P. J. Knowles, G. Knizia, F. R. Manby, M. Schütz, P. Celani, W. Györffy, D. Kats, T. Korona, R. Lindh, A. Mitrushenkov, G. Rauhut, K. R. Shamasundar, T. B. Adler, R. D. Amos, A. Bernhardsson, A. Berning, D. L. Cooper,

M. J. O. Deegan, A. J. Dobbyn, F. Eckert, E. Goll, C. Hampel, A. Hesselmann, G. Hetzer, T. Hrenar, G. Jansen, C. Köppl, Y. Liu, A. W. Lloyd, R. A. Mata, A. J. May, S. J. McNicholas, W. Meyer, M. E. Mura, A. Nicklass, D. P. O'Neill, P. Palmieri, D. Peng, K. Pflüger, R. Pitzer, M. Reiher, T. Shiozaki, H. Stoll, A. J. Stone, R. Tarroni, T. Thorsteinsson and M. Wang, *MOLPRO, Version 2015.1, a Package of ab Initio Programs*, 2015.

46 M. Douglas and N. Kroll, *Ann. Phys.*, 1974, **82**, 89–155.

47 W. D. Allen and . coworkers., 2005, *INTDER* 2005 is a General Program Written by W. D. Allen and Coworkers, which Performs Vibrational Analysis and Higher-Order Non-Linear Transformations.

48 J. F. Gaw, A. Willets, W. H. Green and N. C. Handy, in *Advances in Molecular Vibrations and Collision Dynamics*, ed. J. M. Bowman and M. A. Ratner, JAI Press, Inc., Greenwich, Connecticut, 1991, pp. 170–185.

49 I. M. Mills, in *Molecular Spectroscopy - Modern Research*, ed. K. N. Rao and C. W. Mathews, Academic Press, New York, 1972, pp. 115–140.

50 J. K. G. Watson, in *Vibrational Spectra and Structure*, ed. J. R. During, Elsevier, Amsterdam, 1977, pp. 1–89.

51 D. Papousek and M. R. Aliev, *Molecular Vibration-Rotation Spectra*, Elsevier, Amsterdam, 1982.

52 M. J. Frisch, G. W. Trucks, H. B. Schlegel, G. E. Scuseria, M. A. Robb, J. R. Cheeseman, G. Scalmani, V. Barone, G. A. Petersson, H. Nakatsuji, X. Li, M. Caricato, A. V. Marenich, J. Bloino, B. G. Janesko, R. Gomperts, B. Mennucci, H. P. Hratchian, J. V. Ortiz, A. F. Izmaylov, J. L. Sonnenberg, D. Williams-Young, F. Ding, F. Lipparini, F. Egidi, J. Goings, B. Peng, A. Petrone, T. Henderson, D. Ranasinghe, V. G. Zakrzewski, J. Gao, N. Rega, G. Zheng, W. Liang, M. Hada, M. Ehara, K. Toyota, R. Fukuda, J. Hasegawa, M. Ishida, T. Nakajima, Y. Honda, O. Kitao, H. Nakai, T. Vreven, K. Throssell, J. A. Montgomery, Jr., J. E. Peralta, F. Ogliaro, M. J. Bearpark, J. J. Heyd, E. N. Brothers, K. N. Kudin, V. N. Staroverov, T. A. Keith, R. Kobayashi, J. Normand, K. Raghavachari, A. P. Rendell, J. C. Burant, S. S. Iyengar, J. Tomasi, M. Cossi, J. M. Millam, M. Klene, C. Adamo, R. Cammi, J. W. Ochterski, R. L. Martin, K. Morokuma, O. Farkas, J. B. Foresman and D. J. Fox, *Gaussian~16 Revision C.01*, 2016, Gaussian Inc. Wallingford CT.

53 C. M. Western, *Journal of Quantitative Spectroscopy and Radiative Transfer*, 2017, **186**, 221–242.